RSC Advances

PAPER

View Article Online
View Journal | View Issue

Cite this: *RSC Adv.*, 2018, **8**, 39384

A convenient and efficient precursor transformation route to well-dispersed, stable, and highly accessible supported Au nanocatalysts with excellent catalytic hydrogenation performances†

Jin-Feng Xie,‡[a] Hai-Tao Li,‡[a] Qiang Gao,*[a] Hao Wang[a] and Yan-Sheng Gong*[b]

A new, convenient, and efficient precursor transformation route for the synthesis of supported Au nanocatalysts was reported. In this strategy, $[Au(en)_2]^{3+}$-riched titanate nanospheres (en: ethylenediamine) with hierarchical flower-like architecture were pre-synthesized *via* "ammonia etching-ion exchange" processes and then used as the precursors of the objective catalysts. Direct pyrolysis of these precursors, varying in amount of $[Au(en)_2]^{3+}$, led to the formation of Au nanoparticles (AuNPs) with different contents uniformly supported on highly crystalline titania nanoflowers ($fTiO_2$). The $fTiO_2$-supported AuNPs nanocomposites possessed highly open porous structures with large surface areas (142.3–149.3 $m^2\ g^{-1}$), which could allow guest molecules to diffuse in and out easily. More interestingly, the formed AuNPs with small size (~3.8 nm) were well-dispersed and partially embedded into the nanosheets of $fTiO_2$, which was beneficial for achieving high activity while avoiding their detachment from the support during application. Accordingly, the AuNPs/TiO_2 catalysts exhibited superior catalytic properties for 4-nitrophenol hydrogenation with significantly higher catalytic efficiencies than many previously reported heterogeneous catalysts. Moreover, the catalytic activity could remain almost unchanged after being recycled several times, demonstrating their high stability. These findings open up a new possibility for rational design and synthesis of supported catalysts for diverse catalytic applications.

Received 10th October 2018
Accepted 19th November 2018

DOI: 10.1039/c8ra08379g

rsc.li/rsc-advances

1. Introduction

Supported catalysts, composed of active metal nanoparticles (MNPs) well dispersed on porous supports, represent one of the most important classes of catalysts with special interest for a variety of liquid phase reactions such as hydrogenation, oxidation, and other industrial or environmental applications.[1] Wetness impregnation is the most widely used method for synthesizing such kinds of catalysts, however, either the aggregation of MNPs or their irreversible detachment from the support surfaces during the catalysis process will reduce the catalytic activity and stability, which is also consistently regarded as a major obstacle in the application of the post-loading method to practical synthesis.[2,3] Moreover, the impregnation synthesis of supported MNPs usually requires the use of an excess of reducing reagent (*e.g.*, H_2, $NaBH_4$, and hydrazine), which results in a relatively high production cost and/or reagent waste.[4] This situation entails efforts to develop novel methodology, potentially more effective and economical, for synthesizing active and stable supported catalysts.

Transformations of pre-synthesized solid precursors into morphology-preserved materials has recently emerged as an important new direction in materials chemistry, which will enable possible pathways for the rational design of target materials with a high degree of compositional and structural complexity.[5,6] The versatility of precursor transformation method has been well exemplified in the synthesis of various porous carbon-supported MNPs. Specifically, pyrolysis of structurally defined organometallic coordination polymers or metal–organic frameworks (MOFs) under an inert atmosphere can carbonize the organic fractions and generate MNPs on the surface of as-carbonized matrix.[7,8] One of the advantages of precursor transformation compared to conventional methods is its ability to preserve the morphology and result in a high level of porosity.[9] More importantly, this method can assure homogeneous and firm attachment of MNPs to the carbonaceous matrix, since the MNPs are *in situ* reduced and deposited on the carbonaceous matrix formed almost simultaneously during pyrolysis.[8] However, the resulting supported catalyst typically

[a]*Department of Chemistry, Faculty of Material Science and Chemistry, China University of Geosciences, Wuhan 430074, PR China. E-mail: gaoqiang@cug.edu.cn; Fax: +86 027 6788 3731; Tel: +86 027 6788 3731*

[b]*Department of Materials Science and Engineering, Faculty of Material Science and Chemistry, China University of Geosciences, Wuhan 430074, PR China. E-mail: gongysh@cug.edu.cn*

† Electronic supplementary information (ESI) available. See DOI: 10.1039/c8ra08379g

‡ The two authors contributed equally to this work.

features small pore sizes (<2 nm) and a significant proportion of MNPs are embedded within the pores,[10] which usually makes it difficult for potential reactants to reach the inner active sites and thus leads to a relatively slow reaction rate as compared to exposed catalysts.[11] Therefore, the development of alternative transformation routes to fabricate supported catalysts with highly open porous structures toward facilitating fast molecular diffusion as well as promoting the accessibility of active sites, represents a particularly attractive target in this area.

Precursor design is undoubtedly the critical factor for transformation synthesis of catalyst materials, owing to its central role in controlling material composition and structure. Recently, hydrogen or ammonium titanate with three-dimensional (3D) hierarchical porous structure has aroused considerable interests because of its unique structural characteristics and the potential to be controllably transformed into morphology-preserved crystalline TiO_2 upon thermal treatment.[12–17] For example, Jitputti *et al.* synthesized monodispersed flower-like ammonium titanate nanospheres *via* a simple ammonia etching procedure, and demonstrated that the titanate nanospheres were readily transformed into anatase TiO_2 nanoflowers by calcination in air.[18] Intriguingly, the titanate with highly interconnected 3D hierarchical structures can not only exhibit high specific surface area (>100 $m^2\ g^{-1}$), but possess sufficiently open pathways that can favor fast transportation of guest molecules.[14] Moreover, it can efficiently adsorb metal ions (M^{n+}) from aqueous solution according to the following ion exchange reaction: M^{n+} + $n NH^{4+}$-titanate → M^{n+}-titanate + $n NH^{4+}$.[19] The resulting M^{n+}-titanate integrates the advantages of hierarchical porous structure and M^{n+}-riched surface, which urges us to consider the possibility of using it as an alternative precursor for synthesizing supported catalyst. However, direct pyrolysis of M^{n+}-titanate seems impractical to generate MNPs on the surface of TiO_2 matrix due to the absence of reducing agent. Indeed, the M^{n+}-titanate could be transformed into M^{n+}-doped TiO_2 upon calcination, as demonstrated by our survey and a previous study.[20,21]

Nevertheless, inspired by the advantages of transformation methodology and as our continuing interest in the development of hierarchically structured catalysts, we hypothesize that if the metal ions adsorbed on titanate are substituted by metal–organic complex ions, homogeneously dispersed MNPs might be *in situ* fabricated onto the TiO_2 matrix, because the organic ligand might act as reducing agent during pyrolysis. To realize this design, organic ligand possessing excellent coordination ability toward metal ions is essentially necessary. It is well known that ethylenediamine (en) is one of the most common organic ligands, which can bind strongly a variety of metal ions to form positively charged $[M\text{-}(en)_m]^{n+}$ chelates (m represents the coordination number).[22,23] Therefore, it is speculated that the surface NH^{4+} ions of ammonium titanate should be also replaceable by the $[M\text{-}(en)_m]^{n+}$ species *via* ion exchange, and the resulting $[M\text{-}(en)_m]^{n+}$-riched titanates can be further utilized to synthesize supported catalysts with the desired textures, activities, and stabilities.

Herein, we demonstrate for the first time that transformation reactions using $[M\text{-}(en)_m]^{n+}$-riched titanates as precursors can be successfully exploited to synthesize high-quality supported catalysts. To illustrate this concept, Au nanoparticles (AuNPs) were chosen as model supported metal component because they are the center of great interest in various catalytic reactions.[24–29] Meanwhile, monodispersed flower-like ammonium titanate nanospheres were used as the parent material of hierarchical TiO_2 support. It was verified that the ammonium titanate nanospheres could efficiently capture $[Au(en)_2]^{3+}$ species from $[Au(en)_2]Cl_3$ solution, and then the $[Au(en)_2]^{3+}$-riched titanate nanospheres were readily transformed into highly crystalline TiO_2 nanoflowers-supported AuNPs (AuNPs/fTiO_2) *via* a simple pyrolysis procedure, without the use of any additional reducing reagents. Importantly, benefitting from the inherent advantages of such a precursor, the resulting AuNPs/fTiO_2 composites exhibited hierarchical flower-like porous structure and highly exposed active sites, which were previously difficult to achieve using conventional precursors. Moreover, the Au content could be tunable simply by controlling the initial concentration of $[Au(en)_2]Cl_3$. For catalytic hydrogenation of 4-nitrophenol (4-NP), the novel supported catalysts exhibited high activity, rapid kinetics, and excellent reusability.

2. Experimental

2.1 Chemicals and reagents

Hydrogen tetrachloroaurate(III)hydrate ($HAuCl_4 \cdot 4H_2O$), ethylenediamine (en), concentered ammonium hydroxide ($NH_3 \cdot H_2O$, 28 wt%), ethanol, sodium tetraborohydrate ($NaBH_4$), 4-nitrophenol (4-NP) and were all purchased from Sinopharm Chemical Reagent Co., Ltd. (Shanghai, China). Titanium isopropoxide ($Ti(OC_3H_7)_4$, 98%) was obtained from J&K Scientific Ltd. (Beijing, China). Deionized water was used throughout our experiments.

2.2 Synthesis

General procedure for synthesis of flower-like ammonium titanate. Ammonium titanate nanoflowers were prepared through an ammonia etching process by employing amorphous titania nanospheres as the starting material. Titania nanospheres were obtained *via* a sol–gel approach, according to the reported procedure.[18] Then, 0.9 g of as-prepared amorphous titania nanospheres were dispersed in 105 mL of deionized water. Subsequently, $NH_3 \cdot H_2O$ solution (28 wt%, 15 mL) was added under vigorous stirring. Afterwards, the mixture was sealed in a Teflon-lined stainless-steel autoclave (150 mL) at 120 °C, maintained at this temperature for 12 h, and allowed to be cooled to room temperature. The product was collected by centrifugation, followed by washing with ethanol and water several times. For convenience in discussion, the amorphous titania nanospheres and ammonium titanate nanoflowers were briefly designated as TiO_2 and etched TiO_2, respectively.

General procedure for synthesis of AuNPs/fTiO_2 catalysts. The preparation of AuNPs/fTiO_2 hybrid catalysts involved the following steps. First, the Au source, $[Au(en)_2]Cl_3$, was prepared *via* the reaction of $HAuCl_4$ and ethylenediamine (en) according

to a previously reported procedure.[30] Then, 0.2 g of ammonium titanate nanoflowers (*i.e.*, etched TiO_2) were added to 15 mL of $[Au(en)_2]Cl_3$ solution with a predetermined concentration (0.12, 0.24, 0.36, or 0.48 mg L^{-1}). After stirring at room temperature for 5 h, the solid powders were separated from the solution by centrifugation, washed with ethanol five times, and then dried at 80 °C under vacuum. Finally, the objective products were obtained by calcination at 500 °C for 4 h with a heating rate of 0.5 °C min^{-1}. Corresponding to the gradually increased initial concentrations of $[Au(en)_2]Cl_3$, the products were designated as AuNPs/fTiO_2-I, AuNPs/fTiO_2-II, AuNPs/fTiO_2-III, and AuNPs/fTiO_2-IV, respectively. For comparison, the pure flower-like titania (designated as fTiO_2) without AuNPs loading was also prepared by the same method.

2.3 Characterization

The hierarchical structure and sizes of as-prepared samples were observed by scanning electron microscope (SEM, SU8010, Hitachi, Japan) and transmission electron microscopy (TEM, Philips CM12). X-ray diffraction (XRD) measurements were performed on an X-ray diffractometer (D8-FOCUS, Bruker, Germany) using Cu Kα radiation (λ = 0.15405 nm). X-ray photoelectron spectroscopy (XPS) analysis was conducted on a VG Scientific ESCALAB Mark II spectrometer equipped with two ultra-high vacuum (UHV) chambers. Optical absorbance spectra were obtained using a UV-vis diffuse reflectance spectrometer (UV-vis DRS, UV-2550PC, Shimadzu Co., Japan). N_2 adsorption/desorption measurements were performed on a Micromeritics ASAP2020 surface area analyzer at a liquid nitrogen temperature (77 K). The AuNPs loading amounts were determined with inductively coupled plasma atomic emission spectrometry (ICP-AES, Leeman, USA).

2.4 Catalytic procedures

Catalytic performances of AuNPs/fTiO_2 catalysts were evaluated by catalyzing conversion of 4-nitrophenol (4-NP) to 4-aminophenol (4-AP) in the presence of $NaBH_4$ as the reducing agent. Typically, 0.2 mL of 4-NP solution (5 mmol L^{-1}), 3 mL of $NaBH_4$ solution (0.2 mol L^{-1}), and 6.8 mL of deionized water were added to a standard quartz curette. Subsequently, 5 mg of AuNPs/fTiO_2 powders were introduced to start the reaction under shaking conditions (200 rpm). The reaction temperature was set at 20, 30, or 40 °C, and UV-vis spectra of the solution were recorded at predetermined time intervals to monitor the progress of the reduction reaction.

3. Results and discussion

Scheme 1 depicts the synthetic strategy of well-dispersed, stable, and highly accessible fTiO_2-supported Au nanoparticles (AuNPs/fTiO_2). The flower-like ammonium titanate nanospheres (etched TiO_2) are first synthesized *via* ammonia etching by employing monodispersed amorphous titania nanospheres (TiO_2) as the starting material.[18] Once the ammonium titanate nanospheres are dispersed in $[Au(en)_2]Cl_3$ solution, the surface NH_4^+ ions of ammonium titanate can be easily replaced by the $[Au(en)_2]^{3+}$ species *via* ion exchange. Then, pyrolysis of the $[Au(en)_2]^{3+}$-riched titanate nanospheres can lead to formation of the objective product AuNPs/fTiO_2 with homogeneous distribution of AuNPs on the surface of flower-like titania (fTiO_2), where the ethylenediamine (en) ligand acts as reducing reagent. It is worth noting that the Au content of the AuNPs/fTiO_2 is tunable simply by controlling the initial concentration of $[Au(en)_2]Cl_3$ in solution. At low $[Au(en)_2]Cl_3$ concentration ($\leq$0.24 mg L^{-1}), it was found that all the $[Au(en)_2]^{3+}$ species in solution were completely captured by the ammonium titanate (monitored by ICP-AES), so the actual loading amounts of Au in AuNPs/fTiO_2-I (0.42 wt%) and AuNPs/fTiO_2-II (0.84 wt%) were exactly identical to the theoretical values. When the concentration of $[Au(en)_2]Cl_3$ exceeded 0.36 mg L^{-1}, the solution $[Au(en)_2]^{3+}$ species were found to be incompletely adsorbed by ammonium titanate, which resulted in a slightly lower loading amounts in AuNPs/fTiO_2-III (1.66 wt%) and AuNPs/fTiO_2-IV (3.33 wt%) than the theoretical values (1.68 wt% and 3.36 wt%). To probe whether the physicochemical characteristics of the as-synthesized AuNPs/fTiO_2 composites with different Au contents were satisfactorily developed, multiple analytical techniques including SEM, TEM, XRD, XPS, and N_2 adsorption/desorption measurements were applied.

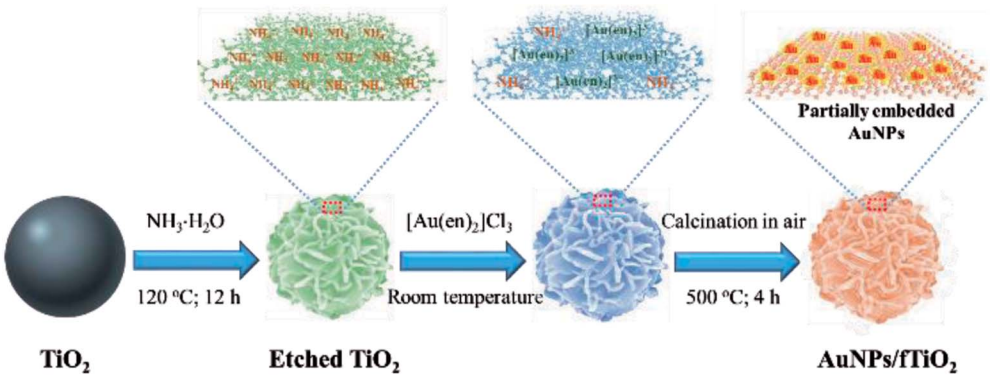

Scheme 1 Synthetic route of the flower-like titania-supported AuNPs (AuNPs/fTiO_2).

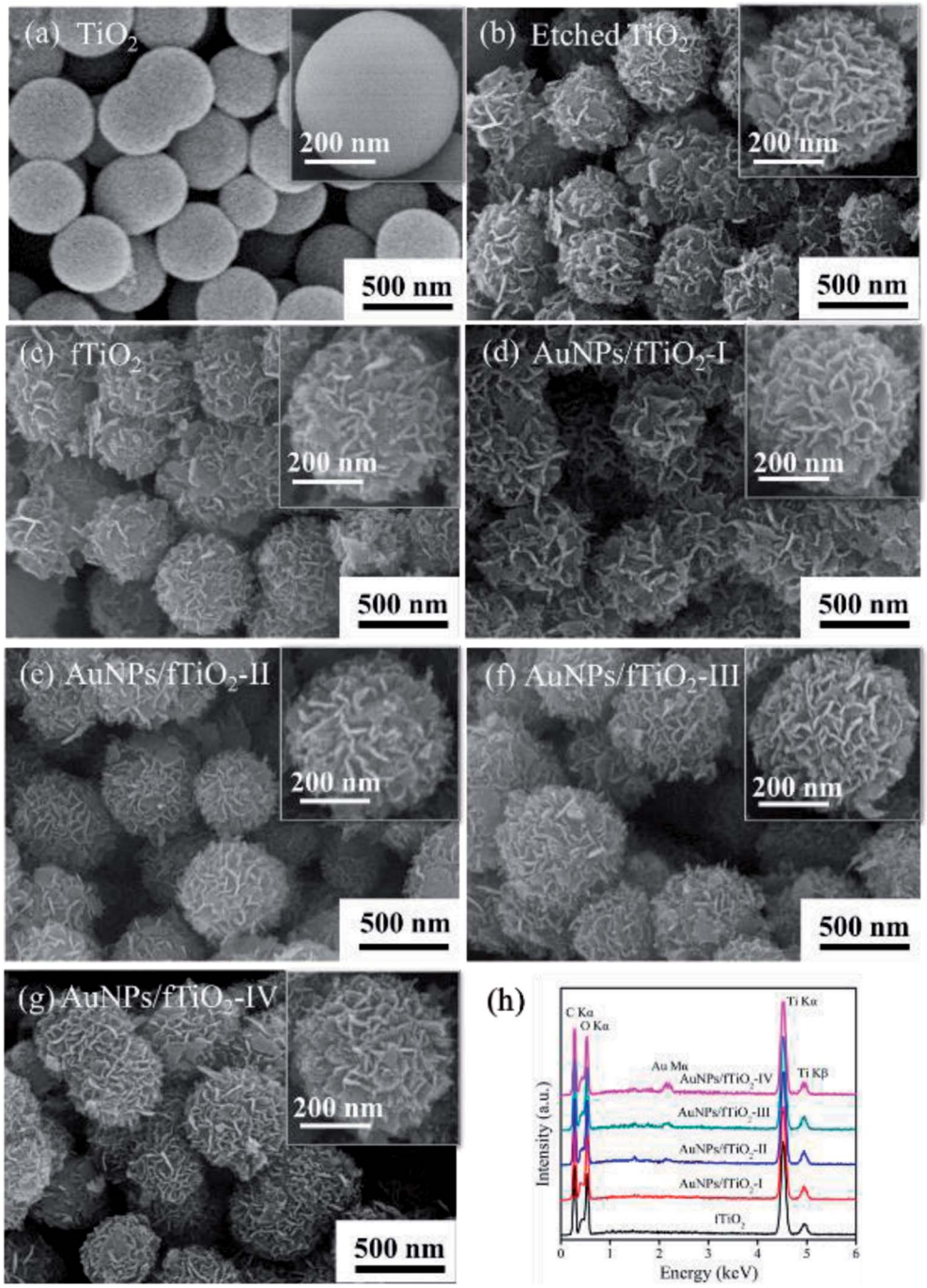

Fig. 1 (a–g) SEM images of the samples involved in this study, and (h) EDS spectra of the flower-like titania samples without and with AuNPs loading.

SEM images were collected for TiO_2, etched TiO_2, $fTiO_2$ (pure titania without AuNPs loading), and AuNPs/$fTiO_2$ samples with different Au contents to distinguish their morphological difference. As seen from Fig. 1a, the TiO_2 sample almost consists of monodispersed and uniform spherical particles with diameters of about 400–500 nm. Upon hydrothermal treatment in ammonia solution at 120 °C for 12 h, these TiO_2 nanospheres were readily etched by ammonia due to their amorphous nature and converted to ammonium titanate ($(NH_4)_2Ti_2O_5 \cdot H_2O$) according to the findings of similar experiments in the literature.[21] The resulting ammonium titanate (*i.e.*, etched titania) shows a unique flower-like architecture that is well organized by many nanosheets (Fig. 1b). Moreover, these nanoflowers also exhibit a high monodispersity, and their diameter is not changed visibly as compared to TiO_2 precursor. Fig. 1c–g show the SEM images of samples ($fTiO_2$, AuNPs/$fTiO_2$-I, AuNPs/$fTiO_2$-II, AuNPs/$fTiO_2$-III, and AuNPs/$fTiO_2$-IV) after calcination at 500 °C for 4 h without and with AuNPs loading. Little morphology difference can be found between the five samples and they are also similar to the etched titania. These

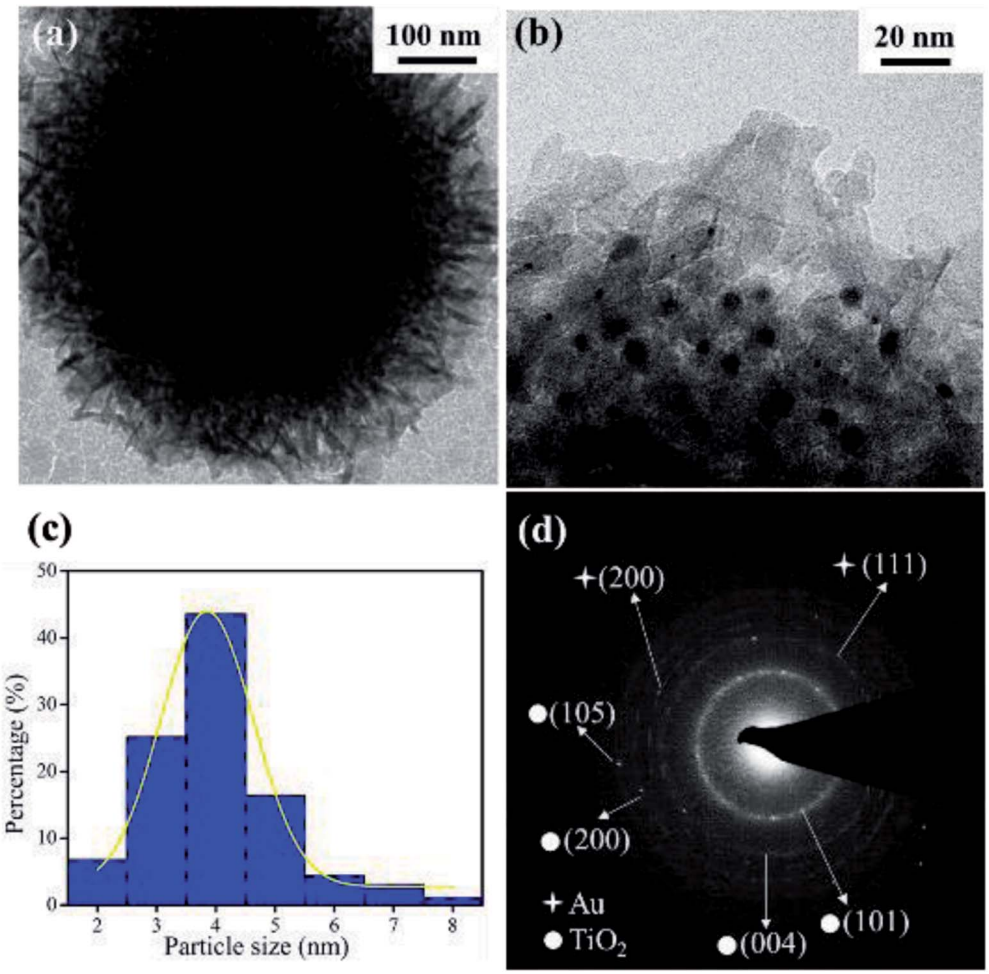

Fig. 2 (a) Low and (b) high resolution TEM images of AuNPs/fTiO$_2$-III, (c) particle size distribution curve, and (d) selected-area electron diffraction (SAED) pattern.

results verify that the nanosheets-assembled flower-like structure can be well maintained during pyrolysis processes. Furthermore, the existence of Au in the four AuNPs/fTiO$_2$ samples was identified by EDS, and the results is shown in Fig. 1h. Evidently, besides Ti and O elements, the Au element can be also found in each AuNPs/fTiO$_2$ sample. Moreover, as expected, the peak intensity of Au element increases with the increase of AuNPs loading amount.

To better illustrate the structure of the supported Au nanocatalysts, representative TEM images taken from the AuNPs/fTiO$_2$-III sample is given in Fig. 2. From Fig. 2a, it can be seen that the AuNPs/fTiO$_2$ particle exhibits a highly open hierarchical flower-like structure assembled by nanosheets. The magnified TEM image (Fig. 2b) clearly shows that ultrafine AuNPs with well-dispersed distribution are uniformly located on the surfaces of nanosheets and no large irregular Au particle is found. The size distribution histogram of AuNPs calculated from the corresponding TEM image is given in Fig. 2c. Clearly, the AuNPs exhibit very small particle sizes (~3.8 nm), which should be active enough for possibly achieving a high catalytic activity.[31,32] More interestingly, the AuNPs do not only decorate the titania nanosheets but are partially embedded within them; thus, the AuNPs/fTiO$_2$ composite is expected to be highly stable during catalytic process. Further analysis of TEM image was conducted using selected area electron diffraction (SAED) (Fig. 2d). The diffraction spots can be assigned to anatase-phased titania ((101), (200), (105), and (004) faces) and cubic-phased Au ((111) and (200) faces),[33,34] respectively, which confirms the successful transformation of $[Au(en)_2]^{3+}$-riched titanate precursor to highly crystalline AuNPs/fTiO$_2$.

Phase structures of fTiO$_2$ and AuNPs/fTiO$_2$ samples were investigated by XRD, and the results are shown in Fig. 3. In pattern of fTiO$_2$ sample, the peaks at 25.3°, 37.8°, 47.9°, 53.9°, 55.0°, and 62.6° can be assigned to the diffractions of (101), (004), (200), (105), (211), and (204) crystalline planes of anatase (JCPDS card no. 04-0477),[35] respectively, and no impurity peaks are found, indicating that the fTiO$_2$ is in a single anatase phase. For each AuNPs/fTiO$_2$ sample, the anatase peaks are still well-resolved and nearly identical to those of fTiO$_2$ sample, which indicates that the crystalline structure of fTiO$_2$ is not influenced by the loading of AuNPs. Besides, the peaks at 38.14°, 44.5°, and 64.7° also appear in their XRD patterns, which can be indexed to the (111), (200), and (220) planes of the Au phase, respectively, according to JCPDS 04-0784.[36] In agreement with above-

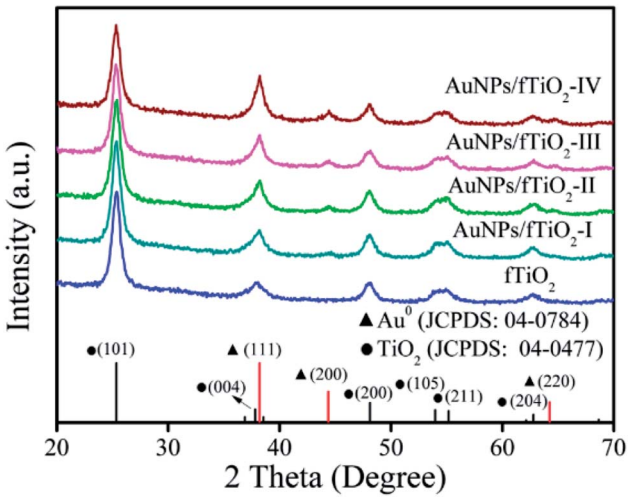

Fig. 3 XRD patterns of the flower-like titania samples without and with AuNPs loading.

discussed EDS result, the intensity of the characteristic peaks of Au phase significantly increases as the loading amount of Au increases. The XRD data further confirm the successful preparation of the AuNPs/$fTiO_2$ catalysts.

The XPS analysis on AuNPs/$fTiO_2$-III was performed to obtain information about the chemical composition of this kind of composites. For comparison, pure titania sample ($fTiO_2$) was also investigated. The elements identified in the survey spectra are Ti, O, and C for both samples, and Au for AuNPs/TiO_2-III, where the C emission peak should be due to the ex situ preparation process or the transfer process of the sample into the UHV chamber (Fig. 4a).[35] The high-resolution Ti XPS spectra of TiO_2 and AuNPs/$fTiO_2$-III exhibit two peaks at 464.4 eV ($2p_{1/2}$) and 458.7 eV ($2p_{3/2}$) (Fig. 4b), which can be assigned to the Ti^{4+} oxidation state according to the reported results.[37] Fig. 4c shows that the binding energies of Au $4f_{7/2}$ and Au $4f_{5/2}$ in AuNPs/TiO_2-III are 83.4 and 87.0 eV, respectively, and the interval value between the two peaks is 3.6 eV, indicating the metallic nature of AuNPs.[38] Compared to the reported results from pure unsupported gold (Au $4f_{7/2}$ = 84.0 eV and Au $4f_{5/2}$ = 87.7 eV),[39] both Au 4f peaks of AuNPs/TiO_2-III shows negative shifts, reflecting the strong interaction of AuNPs with $fTiO_2$ that changes their electronic environment.[38,40] For a supported catalyst, one common disadvantage is that the supported nanoparticles easily come away from the surface of support during use in aqueous media. The presence of strong interaction between AuNPs and $fTiO_2$ might be able to overcome that disadvantage and make the AuNPs/$fTiO_2$ highly stable in catalytic processes.[41–43]

The $fTiO_2$ and AuNPs/$fTiO_2$ samples were further analyzed by Raman and UV-vis DRS spectroscopies. As shown in Fig. 5a, the $fTiO_2$ exhibits modes at 143 cm^{-1} (E_g), 197 cm^{-1} (E_g), 397 cm^{-1} (B_{1g}), 517 cm^{-1} (A_{1g}), and 637 cm^{-1} (E_g), which are characteristic for titania anatase.[44] From the inset of Fig. 5a, it is evident that the anatase E_g absorption mode at 144 cm^{-1} is gradually shifted to higher energies with the increase of Au content, suggesting increased crystalline defects within the anatase

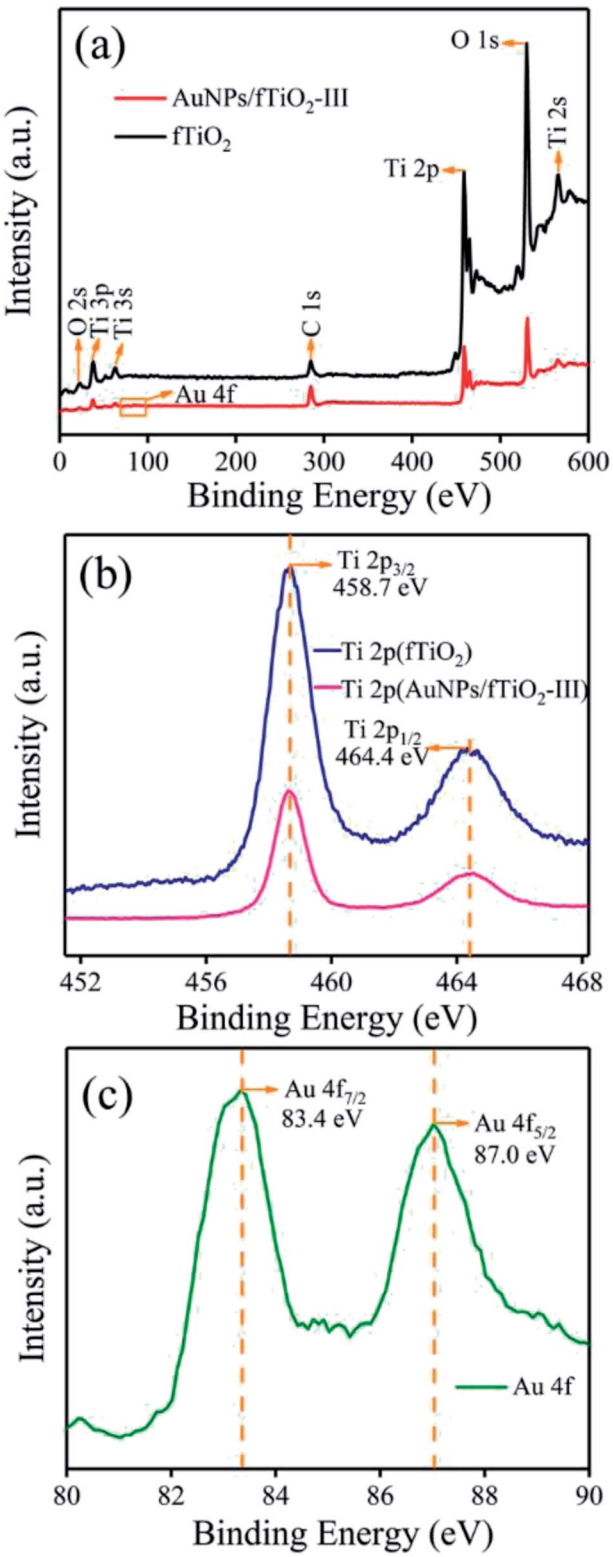

Fig. 4 (a) XPS spectra of $fTiO_2$ and AuNPs/$fTiO_2$-III, (b) Ti 2p spectra of both samples, and (c) Au 4f spectrum of AuNPs/$fTiO_2$-III.

crystal structure.[40] Such defects should be attributed to the partial embedment of AuNPs into titania framework,[45] as demonstrated by TEM image. Fig. 5b shows UV-vis DRS spectra for $fTiO_2$ and four AuNPs/$fTiO_2$ samples. All these samples

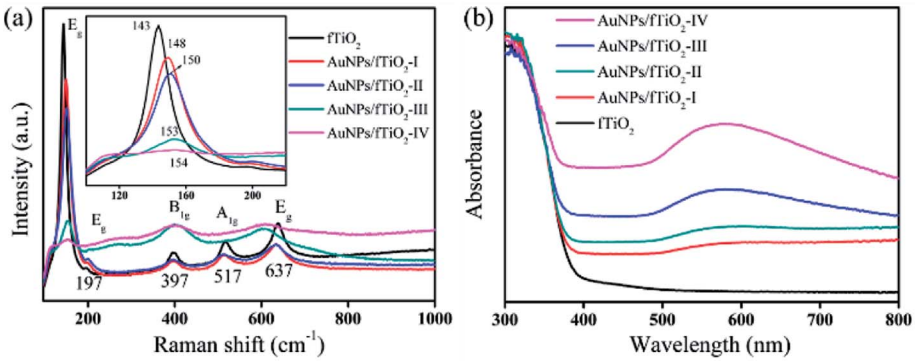

Fig. 5 (a) Raman and (b) UV-vis DRS spectra of the flower-like titania samples without and with AuNPs loading.

exhibit strong absorption below 400 nm due to band gap excitation of anatase matrixes.[46] Besides, the UV-vis DRS spectra of four AuNPs/fTiO$_2$ samples exhibit a significantly enhanced absorption in the visible range (500–600 nm) owing to the plasmon resonance effect of metallic Au, which also indicates the existence of AuNPs.[40] The absorbance intensifies and redshifts with increasing Au loading, which suggests the formation of more and bigger particles.[40]

N_2 adsorption/desorption measurement was conducted to determine the textural parameters of fTiO$_2$ and AuNPs/fTiO$_2$ samples. As shown in Fig. S1a,† the five samples exhibit a type II isotherm pattern with an obvious hysteresis loop, indicating their porous characteristics.[20,47] Moreover, all these samples display an almost identical pore size distribution (obtained by the Barrett–Joyner–Halenda (BJH) method) (Fig. S1b†), which mainly centers at about 6.86 nm, implying that the AuNPs in AuNPs/fTiO$_2$ samples should be largely embedded into the titania skeletons, thereby avoiding pore blocking. The detailed texture parameters are further calculated, and it is found that the surface areas (142.3–149.3 m^2 g^{-1}) and pore volumes (0.39–0.43 cm^3 g^{-1}) of these samples are also very close to each other (Table 1). Compared to some previously developed TiO$_2$-supported AuNPs catalysts (Table S1, ESI†), the AuNPs/fTiO$_2$ catalysts have a larger surface areas and pore volumes. In general, the catalytic performance of a heterogeneous catalyst is positively correlated with its surface area.[48] The large surface area of theses flower-like composites, in conjugation with their highly open structures, distinct crystallinities, and high monodispersity of AuNPs, should be considerably beneficial to their catalytic performances.

The reduction of 4-nitrophenol (4-NP) in the presence of NaBH$_4$ was used as the model reaction to evaluate the catalytic performances of the AuNPs/fTiO$_2$ samples. For comparison, control experiments were first carried out. As shown in Fig. 6a, it can be found that the concentration of 4-NP remains nearly unchanged in the absence of AuNPs/fTiO$_2$, indicating that NaBH$_4$ alone cannot reduce 4-NP under our experiment conditions. When fTiO$_2$ is added to the 4-NP/NaBH$_4$ aqueous solution, the concentration change of 4-NP is still negligible over the investigated period (Fig. 6b), indicating the pure titania material is basically inefficient in catalyzing NaBH$_4$ to generate active hydrogen. In contrast, addition of fTiO$_2$-supported AuNPs into 4-NP/NaBH$_4$ aqueous solution could cause the fading and ultimate bleaching of the yellow color of the 4-NP solution. The processes were monitored by the UV-vis spectrophotometry. Fig. 6c presents the typical spectral results of 4-NP/NaBH$_4$ in the presence of AuNPs/fTiO$_2$-III. It is found that the absorption of 4-NP at 400 nm decreases quickly, along with a concomitant increase of a new peak at 315 nm that can be assigned to 4-aminophenol (4-AP).[49,50] The conversion rate of 4-NP can reach 49.2% within 0.5 min, 80.3% within 2 min, and nearly 100% within 6 min. Moreover, the UV-vis spectra show an isosbestic point between the two absorption bands, indicating that the 4-NP has been specifically converted to 4-AP without any side reaction.[49,50]

To gain insight about the difference of catalytic activities between different AuNPs/fTiO$_2$ catalysts and their temperature-dependent catalytic kinetic behaviors, a series of comparative experiments were further conducted. Considering the concentration of NaBH$_4$ used in our experiments largely exceeds that of 4-NP, the reaction rate can be assumed to be independent of NaBH$_4$ concentration. Therefore, a pseudo-first-order kinetic equation can be applied to evaluate the catalytic rate, which is written as $-dc_t/dt = kc_t$ or $-\ln(c_t/c_0) = kt$, where c_0 and c_t are the initial concentration of 4-NP and its concentration at time t, respectively, and k is the rate constant (min^{-1}).[35] Fig. S2† show the plots of $-\ln(c_t/c_0)$ as a function of t for the reactions respectively catalyzed by AuNPs/fTiO$_2$-I (Fig. S2a†), AuNPs/fTiO$_2$-II (Fig. S2b†), AuNPs/fTiO$_2$-III (Fig. S2c†), and AuNPs/fTiO$_2$-IV (Fig. S2d†) catalysts under different temperatures (20, 30, and 40 °C). According to the linear relationship between $-\ln(c_t/c_0)$ and t, we calculated the rate constants k values from the slopes of the straight lines. In each case, it is found that the rate constant k exhibits an increasing trend with increasing

Table 1 Textural parameters of the flower-like titania samples without and with AuNPs loading

Sample	Surface area (m^2 g^{-1})	Pore size(nm)	Pore volume (cm^3 g^{-1})
fTiO$_2$	145.1	6.86	0.41
AuNPs/fTiO$_2$-I	148.9	6.86	0.43
AuNPs/fTiO$_2$-II	149.3	6.84	0.43
AuNPs/fTiO$_2$-III	146.9	6.86	0.41
AuNPs/fTiO$_2$-IV	142.3	6.88	0.39

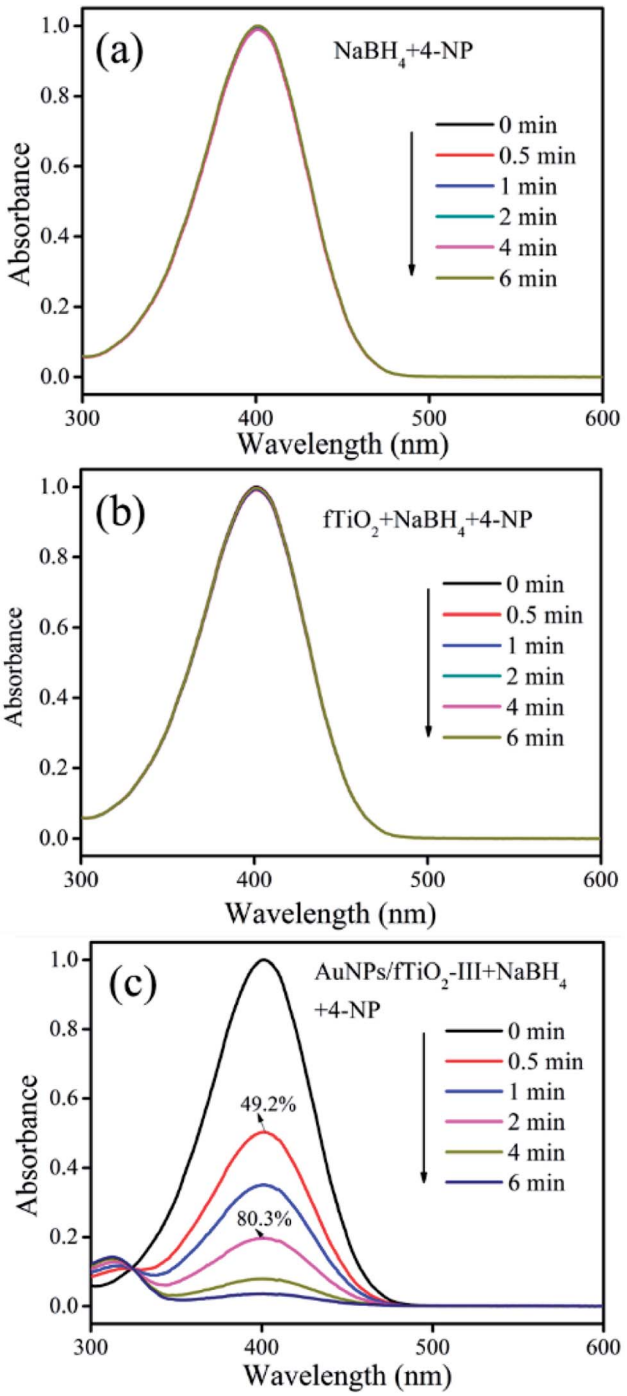

Fig. 6 UV-vis absorption spectra of 4-NP during reduction reactions in the presence of (a) $NaBH_4$ alone, (b) $fTiO_2/NaBH_4$, and (c) AuNPs/$fTiO_2/NaBH_4$, respectively.

temperature. For example, the k value of AuNPs/$fTiO_2$-III-catalyzed reaction is 0.3972 min^{-1} at 20 °C, increases to 0.8887 min^{-1} at 30 °C, and further to 1.2139 min^{-1} at 40 °C (Fig. S2c†), clearly demonstrating that the catalytic efficiency is positively correlated with the reaction temperature. This observation should be understandable because the reducibility of $NaBH_4$ can be enhanced by increasing the reaction temperature, as widely demonstrated in many previous studies.[51]

By comparing the kinetic data obtained from different AuNPs/$fTiO_2$ catalysts under identical temperature condition (Fig. S2†), it can be found that the k value increases firstly and then decreases slightly with the increased content of AuNPs, *i.e.*, AuNPs/$fTiO_2$-I < AuNPs/$fTiO_2$-II < AuNPs/$fTiO_2$-IV < AuNPs/$fTiO_2$-III. For instance, the k values at 30 °C are 0.5630 min^{-1} for AuNPs/$fTiO_2$-I, 0.6084 min^{-1} for AuNPs/$fTiO_2$-II, 0.8887 min^{-1} for AuNPs/$fTiO_2$-III, and 0.7937 min^{-1} for AuNPs/$fTiO_2$-IV, respectively. For the first three samples (*i.e.*, AuNPs/$fTiO_2$-I, AuNPs/$fTiO_2$-II, and AuNPs/$fTiO_2$-III), the persistent increase in catalytic efficiency should be due to the increased loading amount of AuNPs which can provide more active sites for the hydrogenation reaction. When the loading amount of AuNPs further increase (for AuNPs/$fTiO_2$-IV), the catalytic efficiency is slightly poorer than that of AuNPs/$fTiO_2$-III, which should be ascribed to the formation of relatively bigger particles in such case, as revealed by UV-vis DRS results. These findings indicate that a suitable loading amount of AuNPs is crucial for achieving a high catalytic efficiency.

Interestingly, the k value (0.8887 min^{-1}) for AuNPs/$fTiO_2$-III obtained at a common temperature (*e.g.*, 30 °C) is significantly higher than those for many recently reported nanocatalysts, as summarized in Table 2.[52–59] This somewhat indicates the AuNPs/$fTiO_2$-III has outstanding catalytic performance for reduction of 4-NP. Furthermore, the activation energy (E_a) was also calculated from the plots of ln k against $1/T$ according to the Arrhenius equation.[35] The E_a values were estimated to be 40.5 kJ mol^{-1} for AuNPs/$fTiO_2$-I, 41.7 kJ mol^{-1} for AuNPs/$fTiO_2$-II, 42.8 kJ mol^{-1} for AuNPs/$fTiO_2$-III, and 43.6 kJ mol^{-1} for AuNPs/$fTiO_2$-IV, respectively. In general, the E_a values of ordinary chemical reactions are usually between 60 and 250 kJ mol^{-1}.[60] The results presented in this study imply that the catalytic reduction reactions of 4-NP in aqueous solution by our heterogeneous catalytic systems require a lower activation energy and can be easily achieved. Moreover, these values are also significantly lower than those of many previously reported AuNPs-based catalysts, such as magnetically recoverable Au nanocatalyst (51.2 kJ mol^{-1}),[56] Au-based nanoboxes (55.44 ± 3.15 kJ mol^{-1}),[61] and Au/PDDA/NCC (69.2 kJ mol^{-1}),[62] further confirming high catalytic abilities of AuNPs/$fTiO_2$-type catalysts. These results of both activation energies and rate constants indicate the excellent catalytic reduction activities of AuNPs/$fTiO_2$ composites, which should be related closely to their unique features such as highly open structures, high surface areas, large pore volumes, and high dispersion of AuNPs.

Another advantage of AuNPs/$fTiO_2$-type catalysts developed in this work is their high stability. Here, we investigated the cyclic stability of AuNPs/$fTiO_2$-III by reusing the catalyst under identical reaction conditions. As shown in Fig. 7, the catalytic efficiency of AuNPs/$fTiO_2$-III for the reduction of 4-NP remains almost unchanged after five cycles. Compared to the recently reported catalysts such as Ni/SNTs (~20% activity loss after 5 cycles),[63] Cu_2O@h-BN (50% activity loss after 4 cycles),[64] PVPh-Ni_3Co_1 (55% activity loss after 7 cycles),[65] and Ni nanoparticles in hydrogel network (25% activity loss after 5 cycles),[66] our catalyst shows a significantly better durability. The excellent stability of AuNPs/$fTiO_2$-type catalyst should be due to the

Table 2 Comparison of the rate constant k between different catalysts for 4-NP hydrogenation

Sample	Type	k (min^{-1})	Ref.
Pt NFs	Nanoflowers	0.042	52
Pt–Au pNDs/RGOs	Supported bimetallic nanodendrites	0.228	53
Silver/iron oxide	Nanocomposite	0.351	54
H40-PEI-PEG-stabilized AuNPs	Core–shell	0.196	55
Fe_3O_4–Au	Supported nanocomposite	0.381	56
Au–Fe_3O_4	Nanodumbbells	0.63	57
Au@C	Yolk–shell	0.312	58
Fe_3O_4@SiO_2–Au@mSiO_2	Core–shell	0.42	59
AuNPs/fTiO_2-I	Nanoflowers	0.5630	This work
AuNPs/fTiO_2-II	Nanoflowers	0.6084	This work
AuNPs/fTiO_2-III	Nanoflowers	0.8887	This work
AuNPs/fTiO_2-IV	Nanoflowers	0.7937	This work

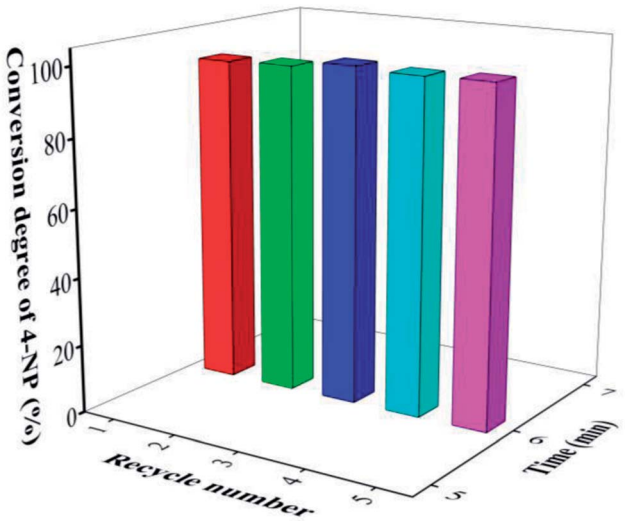

Fig. 7 The reusability of AuNPs/fTiO_2-III catalyst in reduction of 4-NP.

partial embedment of AuNPs into the titania nanosheets, which can effectively avoid detachment from support and prevent their agglomeration under external stimulus.

4. Conclusions

In summary, synthesis of well-dispersed, stable, and highly accessible supported Au nanocatalysts was achieved for the first time *via* a simple and efficient pyrolytic transformation route using $[Au(en)_2]^{3+}$-riched titanate nanoflowers as precursor. The as-prepared AuNPs/fTiO_2 nanocatalysts, composed of AuNPs supported on flower-like titania (fTiO_2), exhibited highly open porous structures with distinct crystallinities and large surface areas (142.3–149.3 m^2 g^{-1}), where the AuNPs were highly dispersed and their loading amount could be predetermined prior to pyrolysis by controlling the $[Au(en)_2]^{3+}$ contents in precursors. More interestingly, the AuNPs did not only decorate the nanosheets of fTiO_2 support but were partially embedded within them, which could avoid pore blocking and prevent their detachment from support. Due to these important characteristics, the AuNPs/fTiO_2 nanocomposites showed excellent catalytic efficiency and high stability for reduction of 4-NP. Through replacing $[Au(en)_2]^{3+}$ with other metal–organic complex ions, we believe that the interesting precursor transformation might be extendable to the fabrication of different supported nanocatalysts with unique structures as well as advanced physical and/or chemical properties.

Conflicts of interest

There are no conflicts to declare.

Acknowledgements

This work was supported by the National Natural Science Foundation of China (No. 21303170) and the Fundamental Research Funds for the Central Universities, China University of Geosciences (Wuhan) (No. CUGL150414, CUGL140413 and CUG120115).

Notes and references

1 G. Prieto, J. Zečević, H. Friedrich, K. Jong and P. Jongh, *Nat. Mater.*, 2013, **12**, 34.
2 H. Liu, L. Zhang, N. Wang and D. Su, *Angew. Chem., Int. Ed.*, 2014, **53**, 12634.
3 Z. Li, J. Liu, Z. Huang, Y. Yang, C. Xia and F. Li, *ACS Catal.*, 2013, **3**, 839.
4 T. Ji, L. Chen, M. Schmitz, F. Bao and J. Zhu, *Green Chem.*, 2015, **17**, 2515.
5 R. Murugavel, M. Walawalkar, M. Dan, H. Roesky and C. Rao, *Acc. Chem. Res.*, 2004, **37**, 763.
6 J. Lee, Y. Sa, T. Kim, H. Moon and S. Joo, *J. Mater. Chem. A*, 2014, **2**, 10435.
7 Y. Yang, Y. Ren, C. Sun and S. Hao, *Green Chem.*, 2014, **16**, 2273.
8 Y. Yang, G. Gao, X. Zhang and F. Li, *ACS Catal.*, 2014, **4**, 1419.
9 X. Xu, R. Cao, S. Jeong and J. Cho, *Nano Lett.*, 2012, **12**, 4988.
10 X. Zhang, G. Ji, W. Liu, B. Quan, X. Liang, C. Shang, Y. Cheng and Y. Du, *Nanoscale*, 2015, **7**, 12932.
11 M. Wang, C. Ye, S. Bao, Z. Chen, Y. Yu, Y. Zhang and M. Xu, *Chem. Commun.*, 2016, **52**, 12992.

12 D. Fattakhova-Rohlfing, A. Zaleska and T. Bein, *Chem. Rev.*, 2014, **114**, 9487.
13 N. Sutradhar, S. Pahari, M. Jayachandran, A. Stephan, J. Nair, B. Subramanian, H. Bajaj, H. Mody and A. Panda, *J. Mater. Chem. A*, 2013, **1**, 9122.
14 M. Feng, W. You, Z. Wu, Q. Chen and H. Zhan, *ACS Appl. Mater. Interfaces*, 2013, **5**, 12654.
15 C. Lin, D. Wong and S. Lu, *ACS Appl. Mater. Interfaces*, 2014, **6**, 16669.
16 H. Wu, X. Lou and H. Hng, *Chem.–Eur. J.*, 2012, **18**, 2094.
17 Y. Takezawa and H. Imai, *Small*, 2006, **2**, 390.
18 J. Jitputti, T. Rattanavoravipa, S. Chuangchote, S. Pavasupree, Y. Suzuki and S. Yoshikawa, *Catal. Commun.*, 2009, **10**, 378.
19 W. Liu, X. Zhao, T. Wang, J. Fu and J. Ni, *J. Mater. Chem. A*, 2015, **3**, 17676.
20 H. Li, Q. Gao, B. Han, Z. Ren, K. Xia and C. Zhou, *ACS Appl. Mater. Interfaces*, 2017, **9**, 371.
21 W. Zhang, W. Zhou, J. Wright, Y. Kim, D. Liu and X. Xiao, *ACS Appl. Mater. Interfaces*, 2014, **6**, 7292.
22 R. Hancock and A. Martell, *Chem. Rev.*, 1989, **89**, 1875.
23 B. Zawisza, A. Baranik, E. Malicka, E. Talik and R. Sitko, *Microchim. Acta*, 2016, **183**, 231.
24 A. Corma and H. Garcia, *Chem. Soc. Rev.*, 2008, **37**, 2096.
25 M. Rudolph and A. Hashmi, *Chem. Soc. Rev.*, 2012, **41**, 2448.
26 W. Zi and F. Toste, *Chem. Soc. Rev.*, 2016, **45**, 4567.
27 J. Fang, B. Zhang, Q. Yao, Y. Yang, J. Xie and N. Yan, *Coord. Chem. Rev.*, 2016, **322**, 1.
28 M. Hülsey, J. Zhang and N. Yan, *Adv. Mater.*, 2018, 1802304.
29 Q. Yao, X. Yuan, T. Chen, D. Leong and J. Xie, *Adv. Mater.*, 2018, 1802751.
30 H. Zhu, C. Liang, W. Yan, S. Overbury and S. Dai, *J. Phys. Chem. B*, 2006, **110**, 10842.
31 M. Daniel and D. Astruc, *Chem. Rev.*, 2004, **104**, 293.
32 S. Cao, J. Chang, L. Fang and L. Wu, *Chem. Mater.*, 2016, **28**, 5596.
33 Z. Jiang, W. Wei, D. Mao, C. Chen, Y. Shi, X. Lv and J. Xie, *Nanoscale*, 2015, **7**, 784.
34 G. Darabdhara, M. Amin, G. Mersal, E. Ahmed, M. Das, M. Zakaria, V. Malgras, S. Alshehri, Y. Yamauchi, S. Szunerits and R. Boukherroub, *J. Mater. Chem. A*, 2015, **3**, 20254.
35 Z. Ren, H. Li, Q. Gao, H. Wang, B. Han, K. Xia and C. Zhou, *Mater. Des.*, 2017, **121**, 167.
36 J. Zhang, Y. Tang, K. Lee and M. Ouyang, *Science*, 2010, **327**, 1634.
37 G. Wang, H. Wang, Y. Ling, Y. Tang, X. Yang, R. Fitzmorris, C. Wang, J. Zhang and Y. Li, *Nano Lett.*, 2011, **11**, 3026.
38 Y. Yu, C. Cao, Z. Chen, H. Liu, P. Li, Z. Dou and W. Song, *Chem. Commun.*, 2013, **49**, 3116.
39 A. Luna, E. Novoseltceva, E. Louarn, P. Beaunier, E. Kowalska and B. Ohtani, *Appl. Catal., B*, 2016, **191**, 18.
40 H. Li, Z. Bian, J. Zhu, Y. Huo, H. Li and Y. Lu, *J. Am. Chem. Soc.*, 2007, **129**, 4538.
41 J. Fang, J. Li, B. Zhang, X. Yuan, H. Asakura, T. Tanaka, K. Teramura, J. Xie and N. Yan, *Nanoscale*, 2015, **7**, 6325.
42 R. Nasaruddin, T. Chen, N. Yan and J. Xie, *Coord. Chem. Rev.*, 2018, **368**, 60.
43 R. Nasaruddin, T. Chen, J. Li, N. Goswami, J. Zhang, N. Yan and J. Xie, *ChemCatChem*, 2018, **10**, 395.
44 A. Sandoval, R. Zanella and T. Klimova, *Catal. Today*, 2017, **282**, 140.
45 S. Farsinezhad, S. Banerjee, B. Rajeeva, B. Wiltshire, H. Sharma, A. Sura, A. Mohammadpour, P. Kar, R. Fedosejevs and K. Shankar, *ACS Appl. Mater. Interfaces*, 2017, **9**, 740.
46 X. Chen and C. Burda, *J. Am. Chem. Soc.*, 2008, **130**, 5018.
47 R. Xiong, C. Lu, Y. Wang, Z. Zhou and X. Zhang, *J. Mater. Chem. A*, 2013, **1**, 14910.
48 Y. Wang, H. Arandiyan, J. Scott, A. Bagheri, H. Dai and R. Amal, *J. Mater. Chem. A*, 2017, **5**, 8825.
49 P. Zhang, Y. Sui, G. Xiao, Y. Wang, C. Wang, B. Liu, G. Zhou and B. Zou, *J. Mater. Chem. A*, 2013, **1**, 1632.
50 Y. Han, X. Wu, X. Zhang, Z. Zhou and C. Lu, *ACS Sustainable Chem. Eng.*, 2016, **4**, 6322.
51 S. Saha, A. Pal, S. Kundu, S. Basu and T. Pal, *Langmuir*, 2010, **26**, 2885.
52 S. Mourdikoudis, T. Altantzis, L. Liz-Marzán, S. Bals, J. Pastoriza-Santos and J. Pérez-Juste, *CrystEngComm*, 2016, **18**, 3422.
53 J. Lv, A. Wang, X. Ma, R. Xiang, J. Chen and J. Feng, *J. Mater. Chem. A*, 2015, **3**, 290.
54 J. Chiou, B. Lai, K. Hsu and D. Chen, *J. Hazard. Mater.*, 2013, **248–249**, 394.
55 Y. Dai, P. Yu, X. Zhang and R. Zhuo, *J. Catal.*, 2016, **337**, 65.
56 Y. Chang and D. Chen, *J. Hazard. Mater.*, 2009, **165**, 664.
57 F. Lin and R. Doong, *J. Phys. Chem. C*, 2011, **115**, 6591.
58 B. Guan, X. Wang, Y. Xiao, Y. Liu and Q. Huo, *Nanoscale*, 2013, **5**, 2469.
59 Y. Deng, Y. Cai, Z. Sun, J. Liu, C. liu, J. Wei, W. Li, C. Liu, Y. Wang and D. Zhao, *J. Am. Chem. Soc.*, 2010, **132**, 8466.
60 Y. Yao, L. Wang, L. Sun, S. Zhu, Z. Huang, Y. Mao, W. Lu and W. Chen, *Chem. Eng. J.*, 2013, **101**, 424.
61 J. Zeng, Q. Zhang, J. Chen and Y. Xia, *Nano Lett.*, 2010, **10**, 30.
62 E. Lam, S. Hrapovic, E. Majid, J. Chong and J. Luong, *Nanoscale*, 2012, **4**, 997.
63 S. Zhang, S. Gai, F. He, S. Ding, L. Li and P. Yang, *Nanoscale*, 2014, **6**, 11181.
64 C. Huang, W. Ye, Q. Liu and X. Qiu, *ACS Appl. Mater. Interfaces*, 2014, **6**, 14469.
65 M. Raula, M. Rashid, S. Lai, M. Roy and T. Mandal, *ACS Appl. Mater. Interfaces*, 2012, **4**, 878.
66 N. Sahiner, H. Ozay, O. Ozay and N. Aktas, *Appl. Catal., A*, 2010, **385**, 201.